Supporting Information: Targeted Teleconnections and their Application to the Postprocessing of Climate Predictions

Clementine Dalelane, Andreas Paxian, Martín Senande, Sabela Sanfiz, Estéban Rodríguez Guisado, Jan Wandel, Abhinav Tyagi

July 2025

Contents

- Figure S1: North–Atlantic European seasonal teleconnection patterns. Untargeted MSLP (EOF), PR-targeted MSLP, and respective PR-patterns.
- Figure S2 to S13: MSESS of seasonal T2M GCFS2.1 hindcasts initialized in January to December. Ensemble mean; Subensemble mean based on true untargeted teleconnctions; Subensemble mean based on true T2M-targeted teleconnections; Subensemble mean based on empirically predicted T2M-targeted teleconnections.
- Figure S14 to S25: MSESS of seasonal PR GFCS2.1 hindcasts initialized in January to December. Ensemble mean; Ensemble mean downscaled with EOF teleconnctions; Subensemble mean based on empirical prediction of T2M-targeted teleconnections, downscaled with untargeted teleconnections; Subensemble mean based on empirical prediction of T2M-targetd teleconnections, downscaled with PR-targeted teleconnections.
- Figure S26 and S27: Differences in T2M and PR skill between the ensemble weighted wrt. EOFs and the RAW one. Averaged difference of Spearman Rank correlation (computed between ensemble mean and ERA5 anomalies for each grid point, and for each of the ensembles) over the domain between 36° and 44° N, 9° W and 3° E.
- Figure S28 and S29: Differences in T2M and PR skill between the ensemble weighted wrt. PLS modes and the RAW one. Averaged difference of Spearman Rank correlation (computed between ensemble mean and ERA5 anomalies for each grid point, and for each of the ensembles) over the domain between 36° and 44° N, 9° W and 3° E.

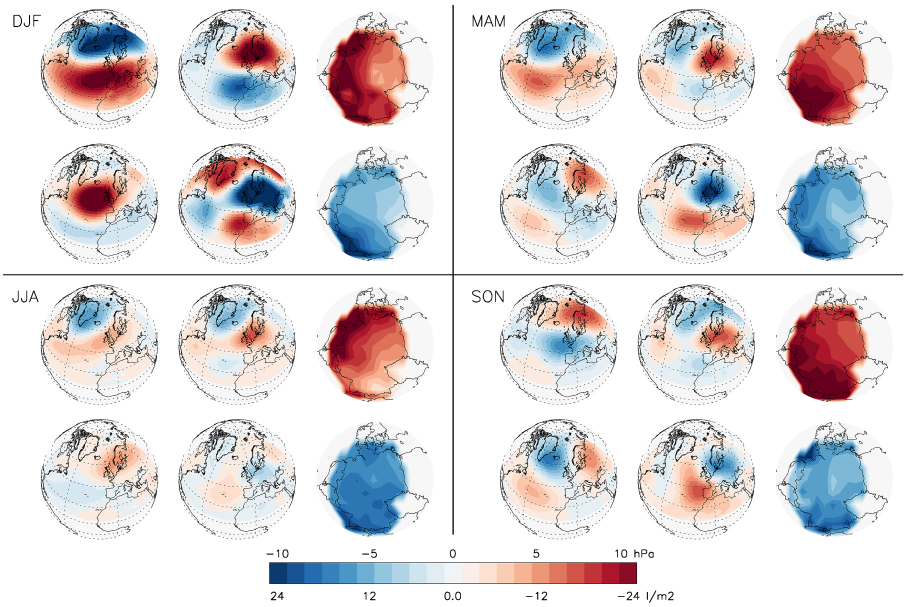

Figure S1: North–Atlantic European seasonal teleconnection patterns. Seasonal subplots left/center/right colums: untargeted MSLP (EOF)/PR-targeted MSLP/respective PR-patterns. Upper/lower rows: first/second dominant patterns.

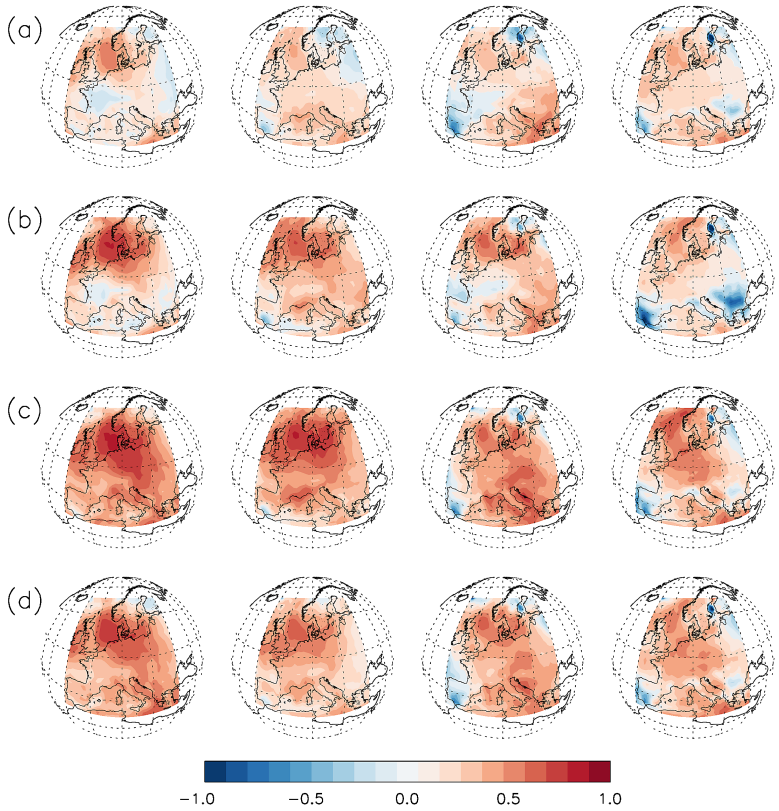

Figure S2: MSESS of seasonal T2M GCFS2.1 hindcasts initialized in January. (a) ensemble mean; (b) subensemble mean based on true untargeted teleconnctions; (c) subensemble mean based on true T2M-targeted teleconnections; (d) subensemble mean based on empirically predicted T2M-targeted teleconnections. Left to right: lead times JFM to AMJ.

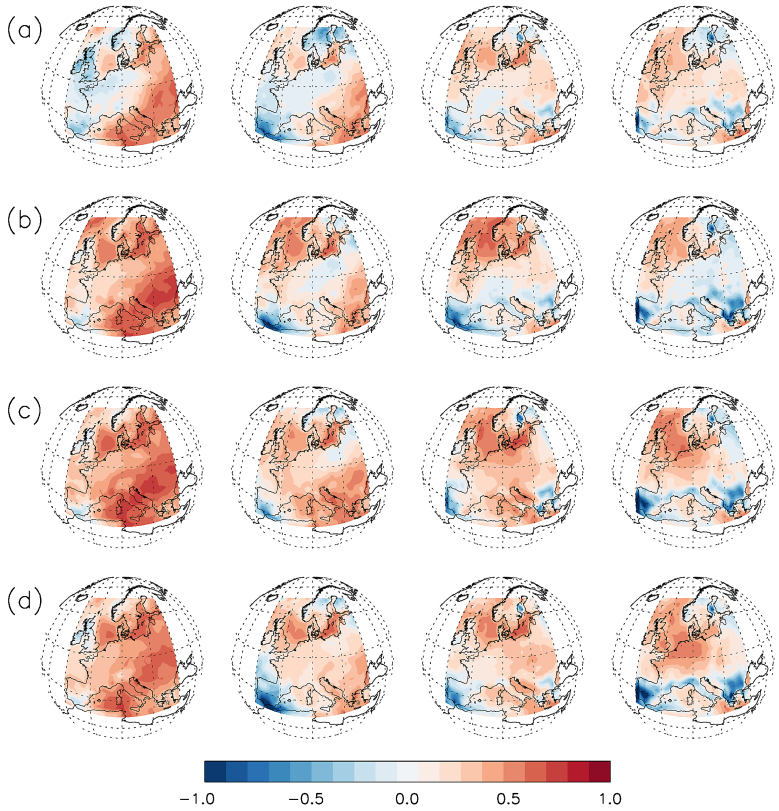

Figure S3: MSESS of seasonal T2M GCFS2.1 hindcasts initialized in February. (a) ensemble mean; (b) subensemble mean based on true untargeted teleconnctions; (c) subensemble mean based on true T2M-targeted teleconnections; (d) subensemble mean based on empirically predicted T2M-targeted teleconnections. Left to right: lead times FMA to MJJ.

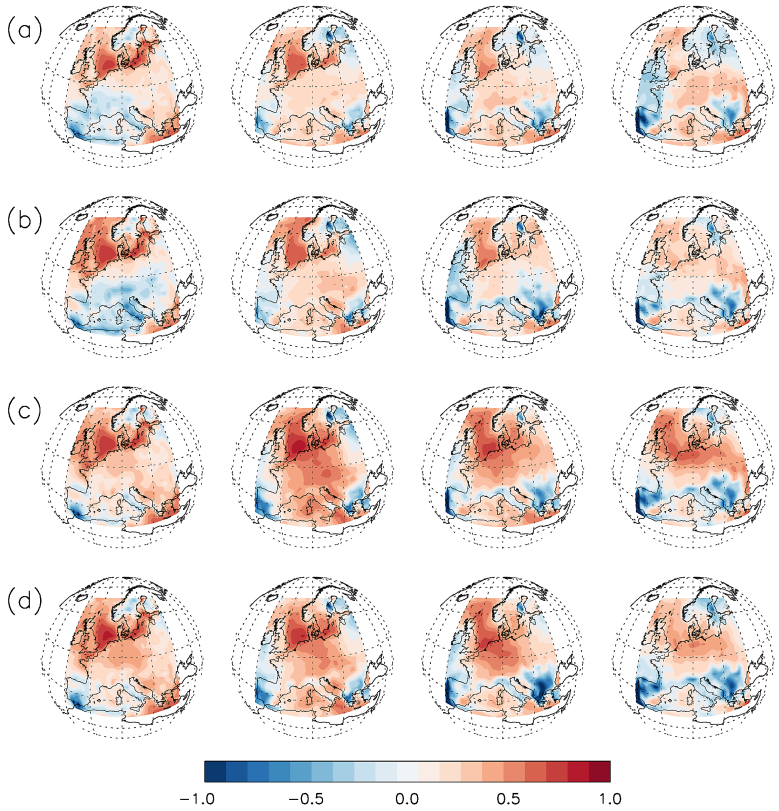

Figure S4: MSESS of seasonal T2M GCFS2.1 hindcasts initialized in March. (a) ensemble mean; (b) subensemble mean based on true untargeted teleconnctions; (c) subensemble mean based on true T2M-targeted teleconnections; (d) subensemble mean based on empirically predicted T2M-targeted teleconnections. Left to right: lead times MAM to JJA.

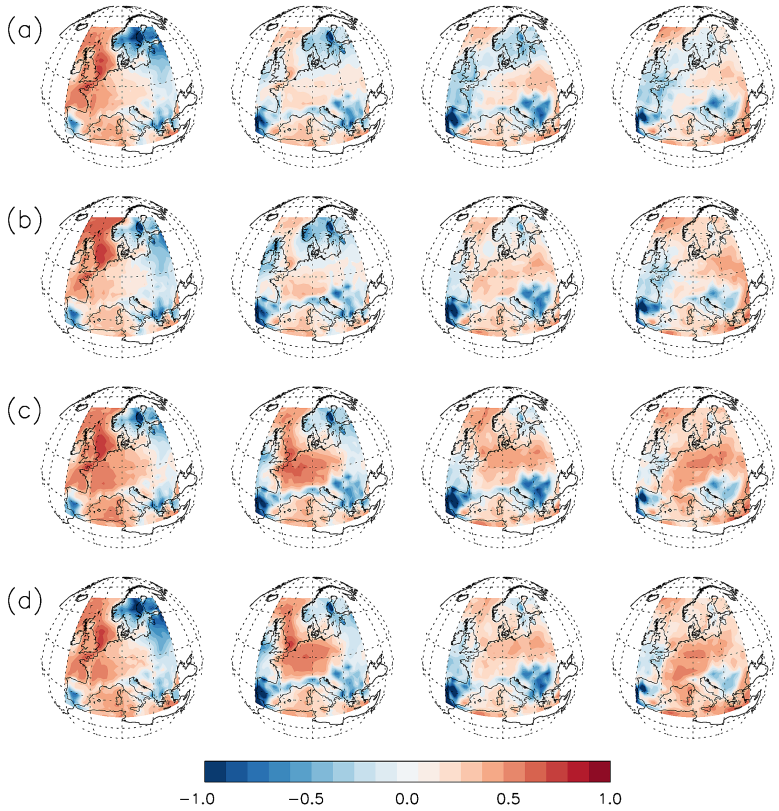

Figure S5: MSESS of seasonal T2M GCFS2.1 hindcasts initialized in April. (a) ensemble mean; (b) subensemble mean based on true untargeted teleconnctions; (c) subensemble mean based on true T2M-targeted teleconnections; (d) subensemble mean based on empirically predicted T2M-targeted teleconnections. Left to right: lead times AMJ to JAS.

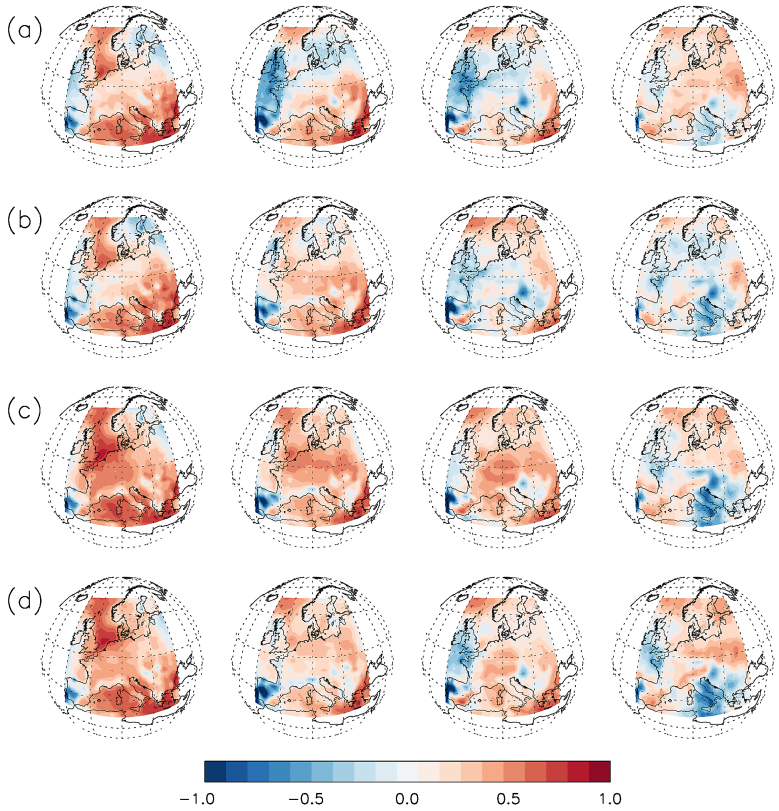

Figure S6: MSESS of seasonal T2M GCFS2.1 hindcasts initialized in May. (a) ensemble mean; (b) subensemble mean based on true untargeted teleconnections; (c) subensemble mean based on true T2M-targeted teleconnections; (d) subensemble mean based on empirically predicted T2M-targeted teleconnections. Left to right: lead times MJJ to ASO.

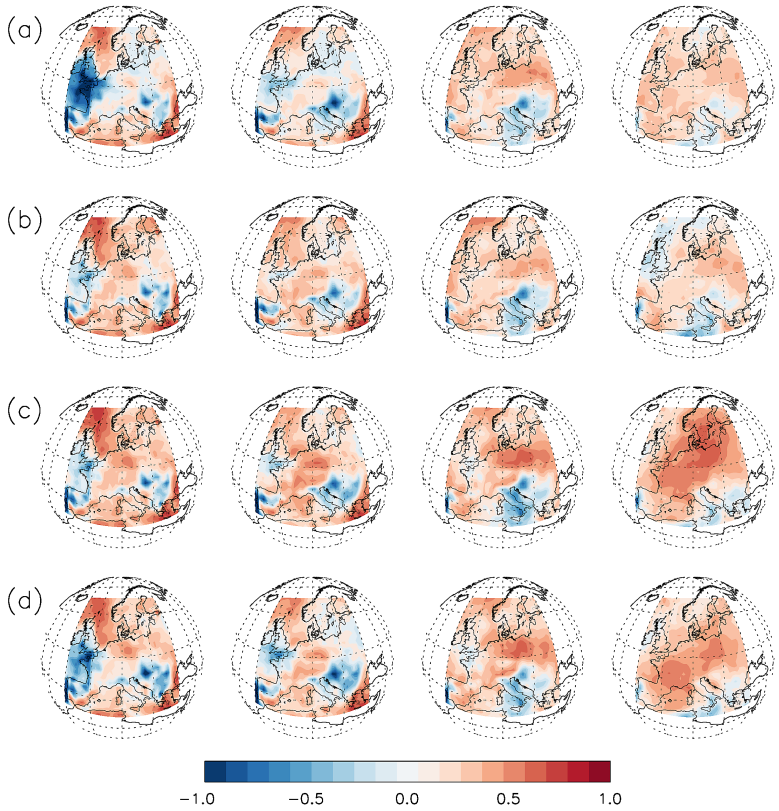

Figure S7: MSESS of seasonal T2M GCFS2.1 hindcasts initialized in June. (a) ensemble mean; (b) subensemble mean based on true untargeted teleconnctions; (c) subensemble mean based on true T2M-targeted teleconnections; (d) subensemble mean based on empirically predicted T2M-targeted teleconnections. Left to right: lead times JJA to SON.

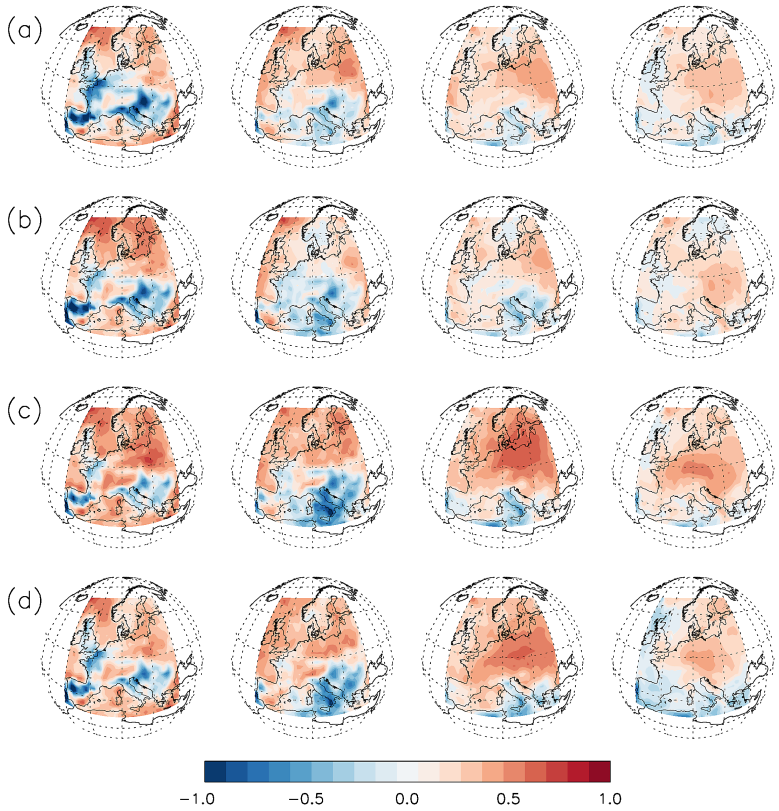

Figure S8: MSESS of seasonal T2M GCFS2.1 hindcasts initialized in July. (a) ensemble mean; (b) subensemble mean based on true untargeted teleconnections; (c) subensemble mean based on true T2M-targeted teleconnections; (d) subensemble mean based on empirically predicted T2M-targeted teleconnections. Left to right: lead times JAS to OND.

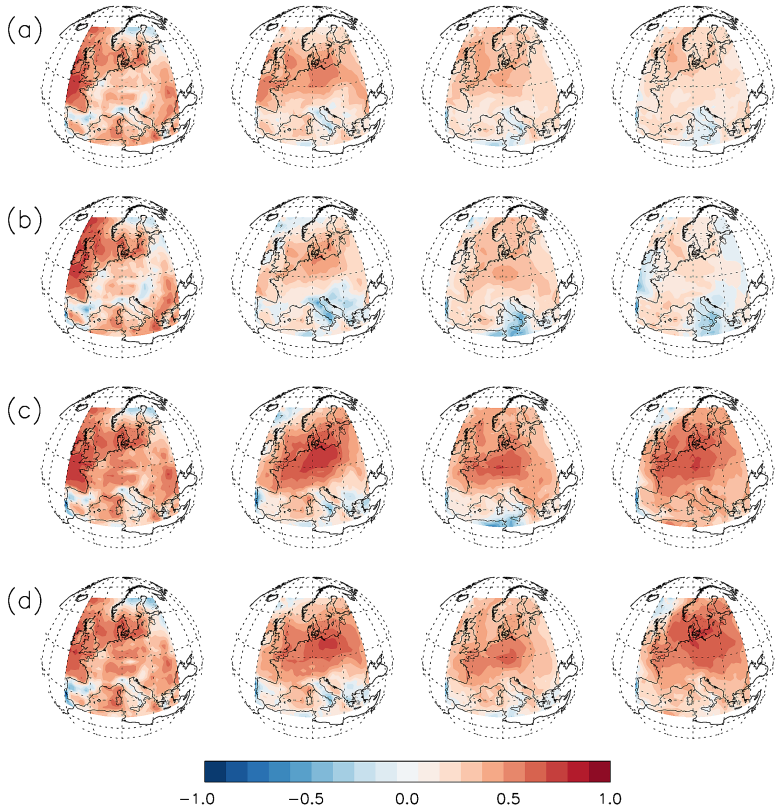

Figure S9: MSESS of seasonal T2M GCFS2.1 hindcasts initialized in August. (a) ensemble mean; (b) subensemble mean based on true untargeted teleconnctions; (c) subensemble mean based on true T2M-targeted teleconnections; (d) subensemble mean based on empirically predicted T2M-targeted teleconnections. Left to right: lead times ASO to NDJ.

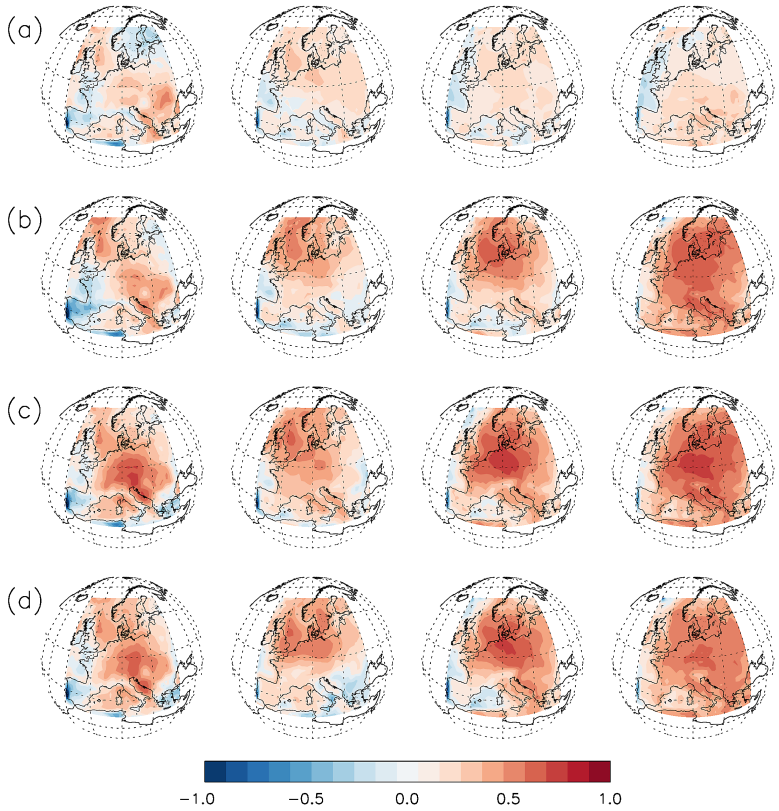

Figure S10: MSESS of seasonal T2M GCFS2.1 hindcasts initialized in September. (a) ensemble mean; (b) subensemble mean based on true untargeted teleconnctions; (c) subensemble mean based on true T2M-targeted teleconnections; (d) subensemble mean based on empirically predicted T2M-targeted teleconnections. Left to right: lead times SON to DJF.

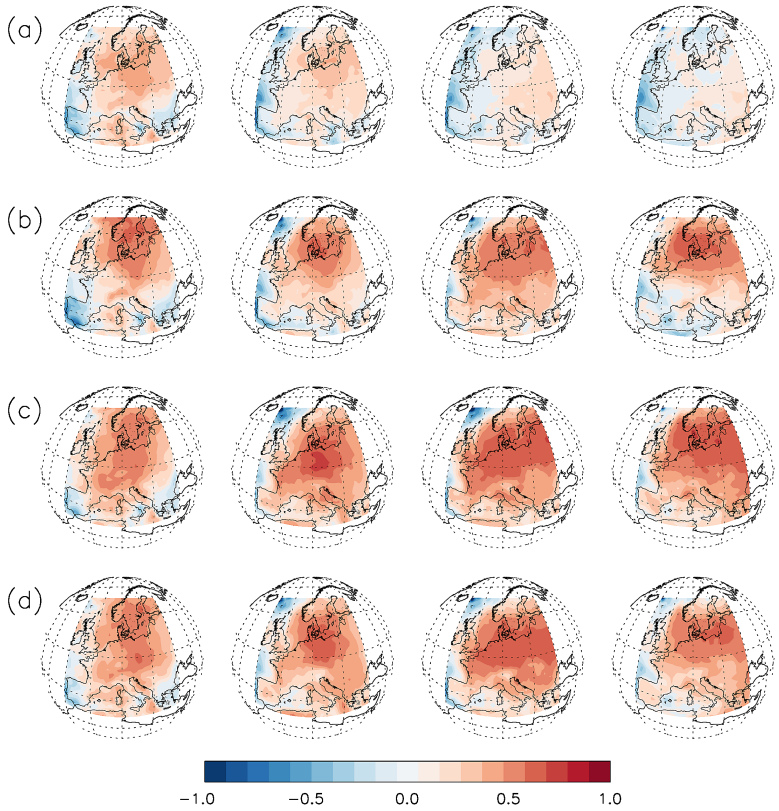

Figure S11: MSESS of seasonal T2M GCFS2.1 hindcasts initialized in October. (a) ensemble mean; (b) subensemble mean based on true untargeted teleconnctions; (c) subensemble mean based on true T2M-targeted teleconnections; (d) subensemble mean based on empirically predicted T2M-targeted teleconnections. Left to right: lead times OND to JFM.

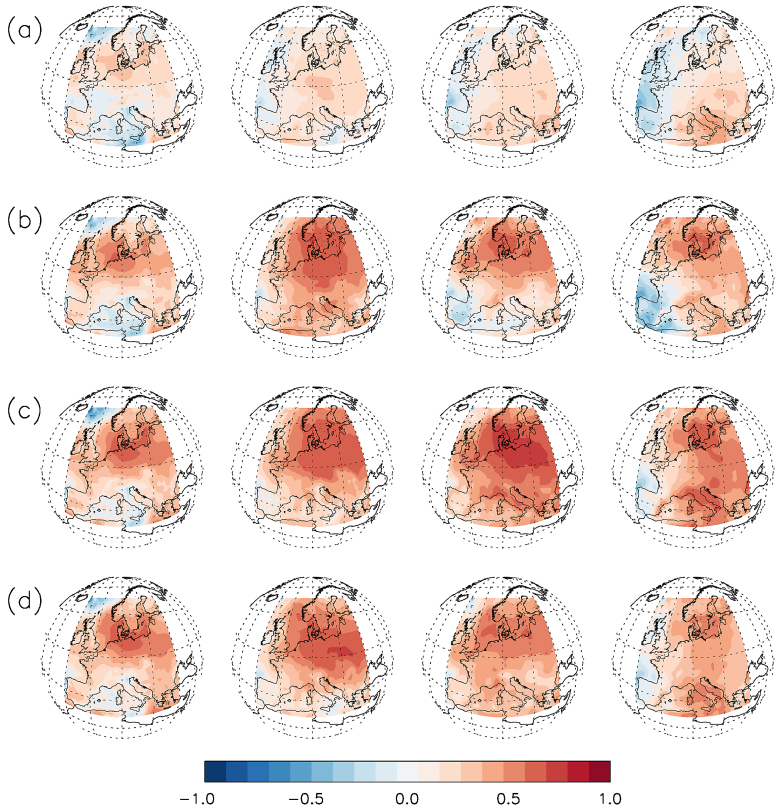

Figure S12: MSESS of seasonal T2M GCFS2.1 hindcasts initialized in November. (a) ensemble mean; (b) subensemble mean based on true untargeted teleconnctions; (c) subensemble mean based on true T2M-targeted teleconnections; (d) subensemble mean based on empirically predicted T2M-targeted teleconnections. Left to right: lead times NDJ to FMA.

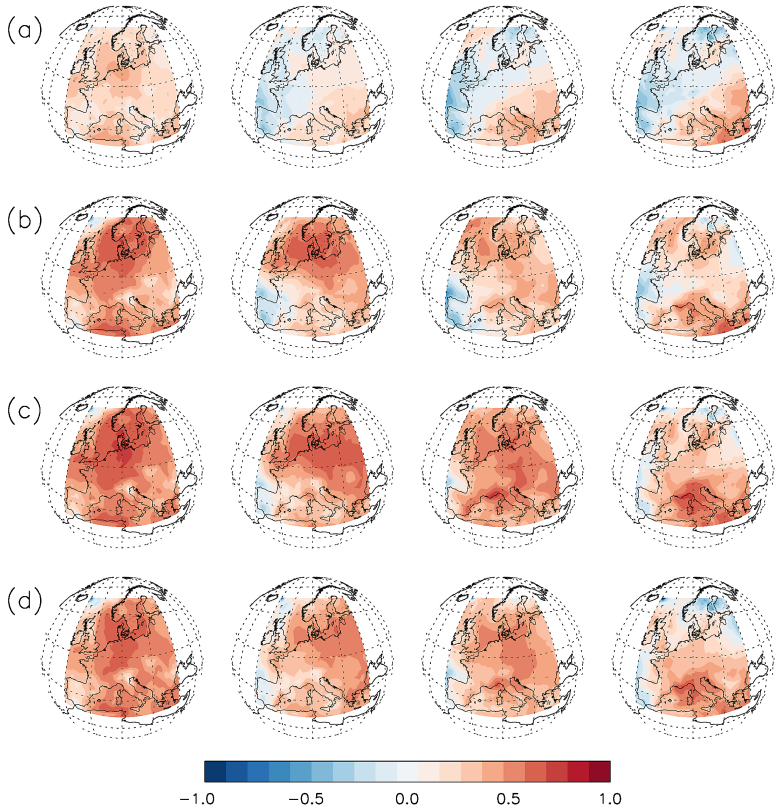

Figure S13: MSESS of seasonal T2M GCFS2.1 hindcasts initialized in December. (a) ensemble mean; (b) subensemble mean based on true untargeted teleconnctions; (c) subensemble mean based on true T2M-targeted teleconnections; (d) subensemble mean based on empirically predicted T2M-targeted teleconnections. Left to right: lead times DJF to MAM.

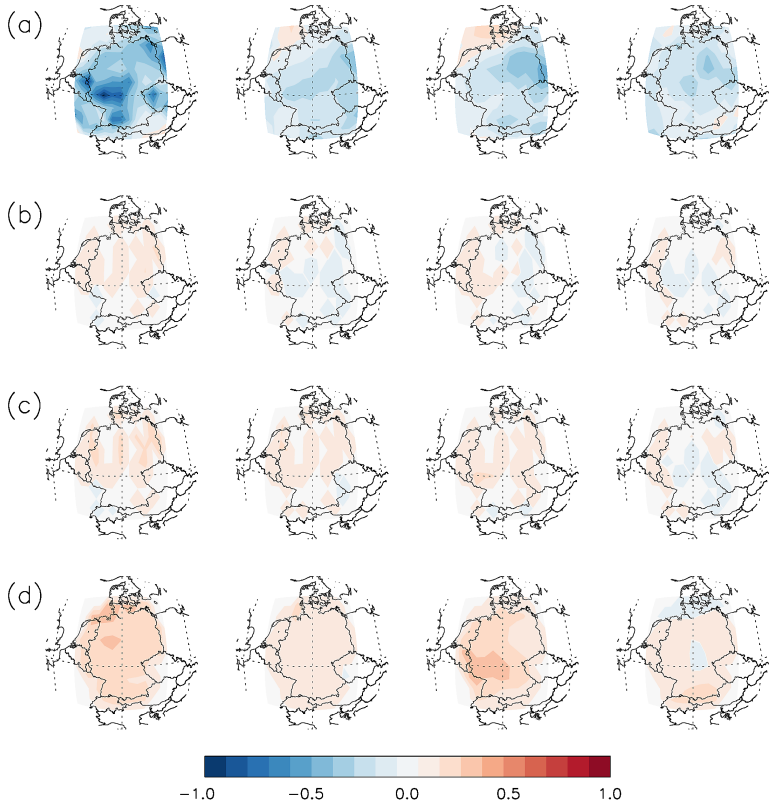

Figure S14: MSESS of seasonal PR GFCS2.1 hindcasts initialized in January. (a) ensemble mean; (b) ensemble mean downscaled with EOF teleconnctions; (c) subensemble mean based on empirical prediction of T2M-targeted teleconnections, downscaled with untargeted teleconnections; (d) subensemble mean based on empirical prediction of T2M-targetd teleconnections, downscaled with PR-targeted teleconnections. Left to right: lead times JFM to AMJ.

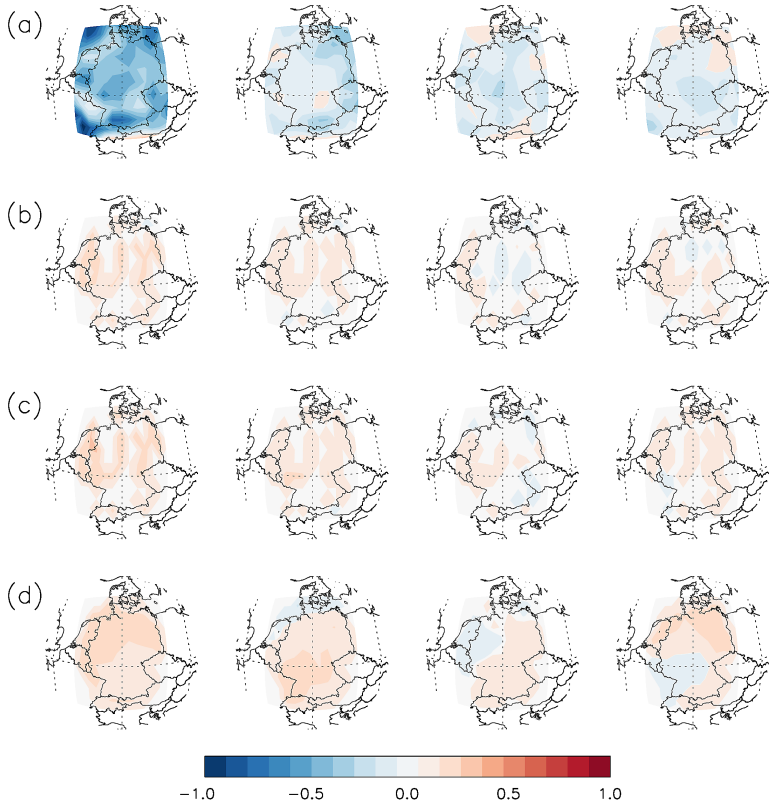

Figure S15: MSESS of seasonal PR GFCS2.1 hindcasts initialized in February. (a) ensemble mean; (b) ensemble mean downscaled with EOF teleconnctions; (c) subensemble mean based on empirical prediction of T2M-targeted teleconnections, downscaled with untargeted teleconnections; (d) subensemble mean based on empirical prediction of T2M-targetd teleconnections, downscaled with PR-targeted teleconnections. Left to right: lead times FMA to MJJ.

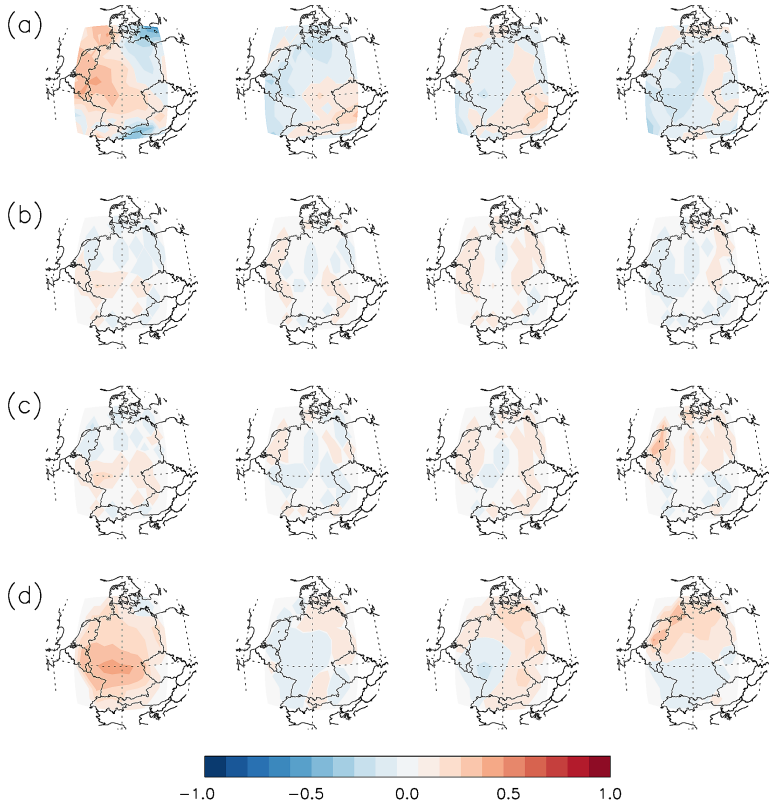

Figure S16: MSESS of seasonal PR GFCS2.1 hindcasts initialized in March. (a) ensemble mean; (b) ensemble mean downscaled with EOF teleconnctions; (c) subensemble mean based on empirical prediction of T2M-targeted teleconnections, downscaled with untargeted teleconnections; (d) subensemble mean based on empirical prediction of T2M-targetd teleconnections, downscaled with PR-targeted teleconnections. Left to right: lead times MAM to JJA.

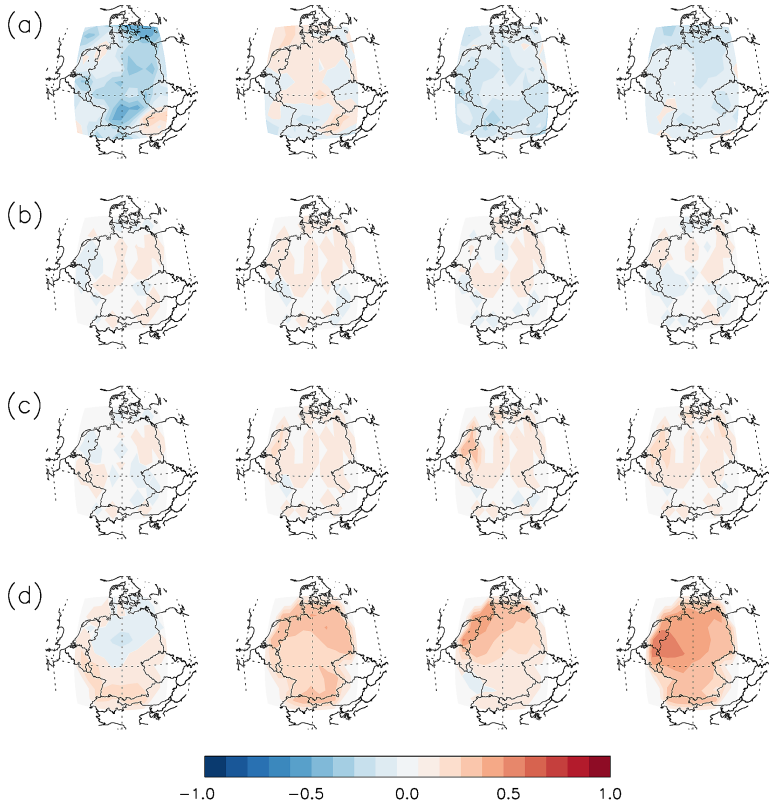

Figure S17: MSESS of seasonal PR GFCS2.1 hindcasts initialized in April. (a) ensemble mean; (b) ensemble mean downscaled with EOF teleconnctions; (c) subensemble mean based on empirical prediction of T2M-targeted teleconnections, downscaled with untargeted teleconnections; (d) subensemble mean based on empirical prediction of T2M-targetd teleconnections, downscaled with PR-targeted teleconnections. Left to right: lead times AMJ to JAS.

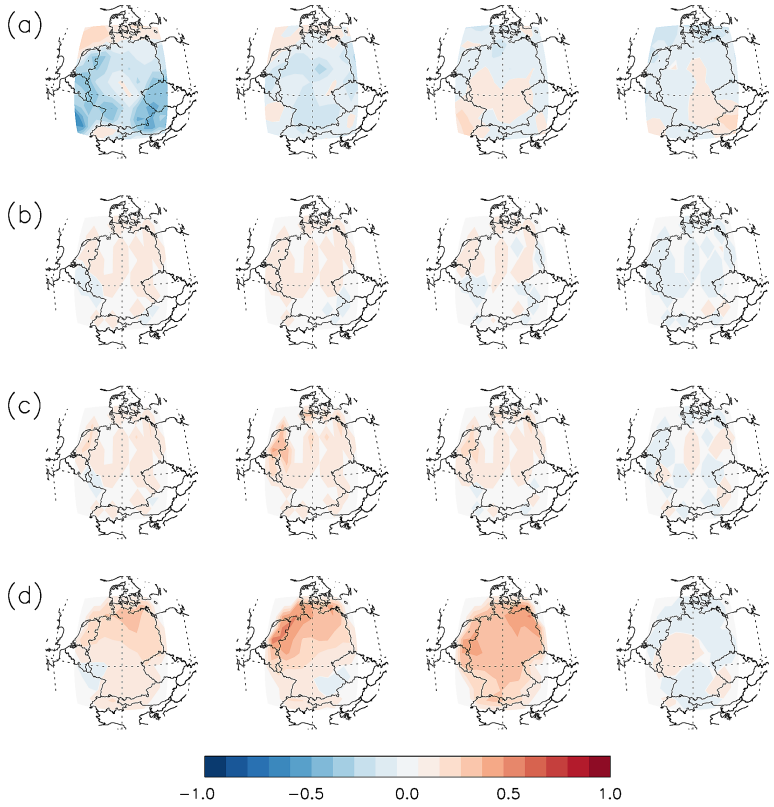

Figure S18: MSESS of seasonal PR GFCS2.1 hindcasts initialized in May. (a) ensemble mean; (b) ensemble mean downscaled with EOF teleconnctions; (c) subensemble mean based on empirical prediction of T2M-targeted teleconnections, downscaled with untargeted teleconnections; (d) subensemble mean based on empirical prediction of T2M-targetd teleconnections, downscaled with PR-targeted teleconnections. Left to right: lead times MJJ to ASO.

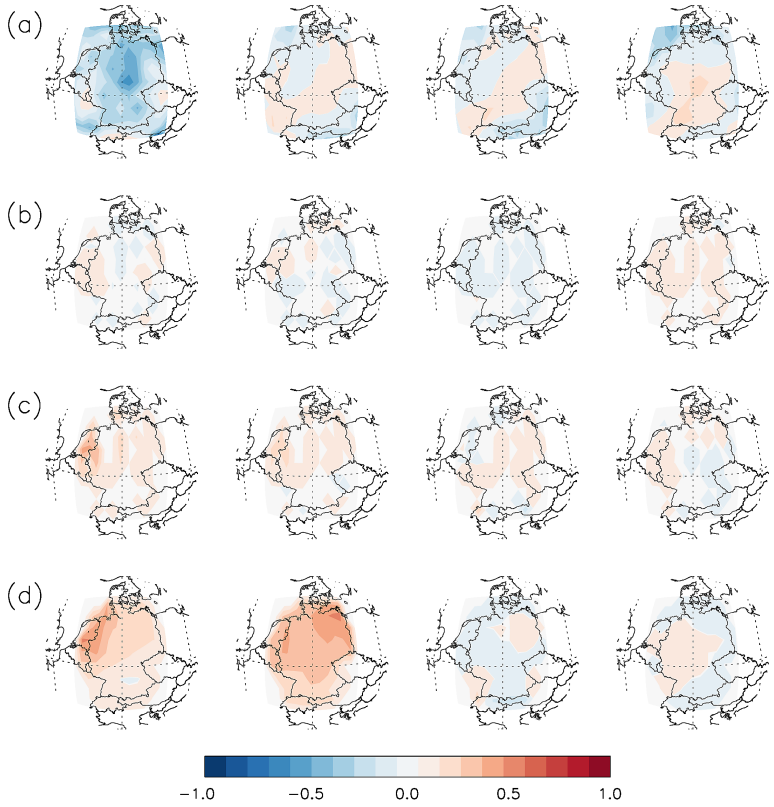

Figure S19: MSESS of seasonal PR GFCS2.1 hindcasts initialized in June. (a) ensemble mean; (b) ensemble mean downscaled with EOF teleconnctions; (c) subensemble mean based on empirical prediction of T2M-targeted teleconnections, downscaled with untargeted teleconnections; (d) subensemble mean based on empirical prediction of T2M-targetd teleconnections, downscaled with PR-targeted teleconnections. Left to right: lead times JJA to SON.

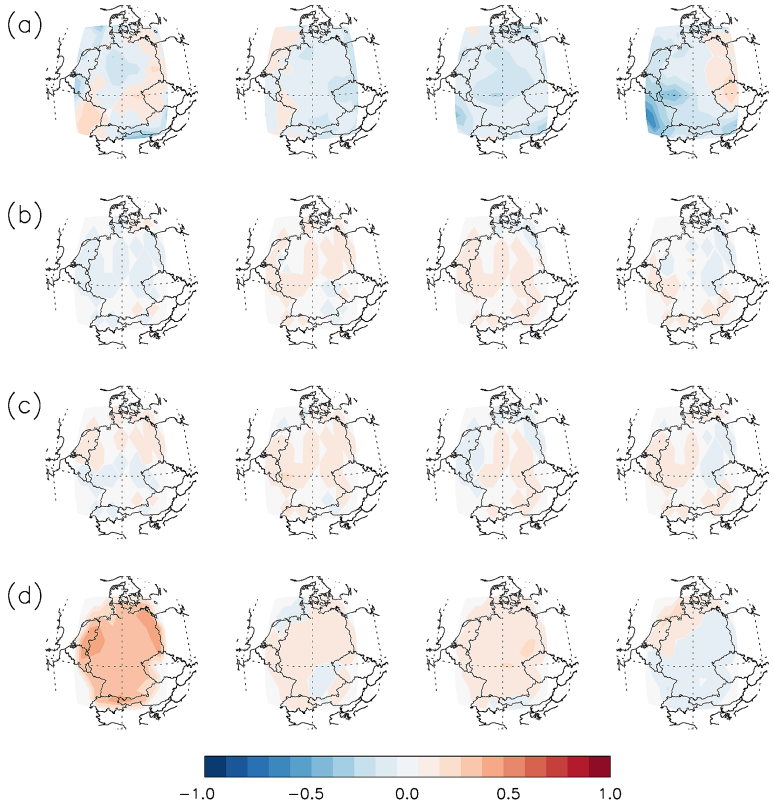

Figure S20: MSESS of seasonal PR GFCS2.1 hindcasts initialized in July. (a) ensemble mean; (b) ensemble mean downscaled with EOF teleconnctions; (c) subensemble mean based on empirical prediction of T2M-targeted teleconnections, downscaled with untargeted teleconnections; (d) subensemble mean based on empirical prediction of T2M-targetd teleconnections, downscaled with PR-targeted teleconnections. Left to right: lead times JAS to OND.

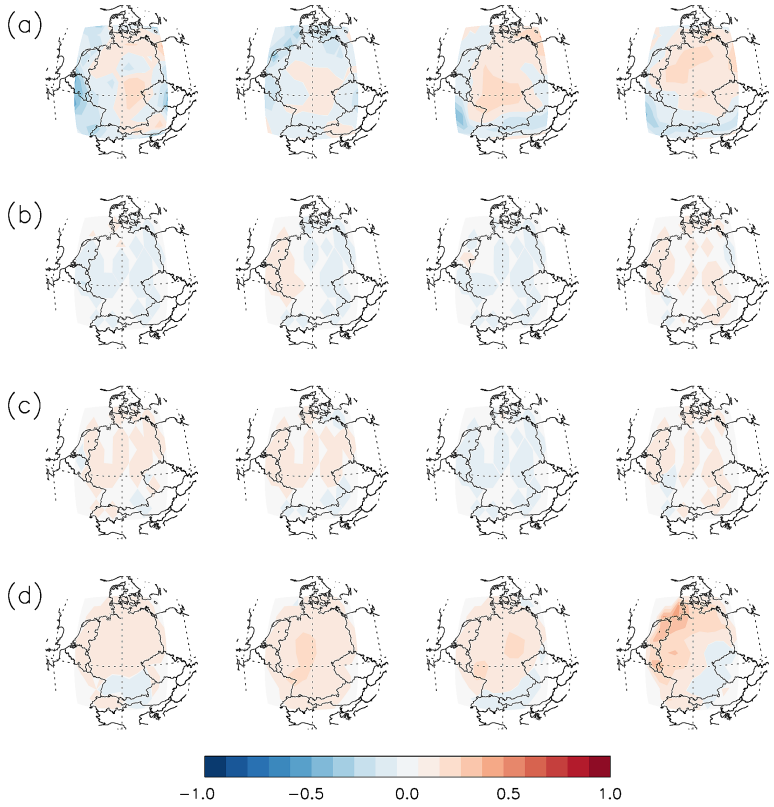

Figure S21: MSESS of seasonal PR GFCS2.1 hindcasts initialized in August. (a) ensemble mean; (b) ensemble mean downscaled with EOF teleconnctions; (c) subensemble mean based on empirical prediction of T2M-targeted teleconnections, downscaled with untargeted teleconnections; (d) subensemble mean based on empirical prediction of T2M-targetd teleconnections, downscaled with PR-targeted teleconnections. Left to right: lead times ASO to NDJ.

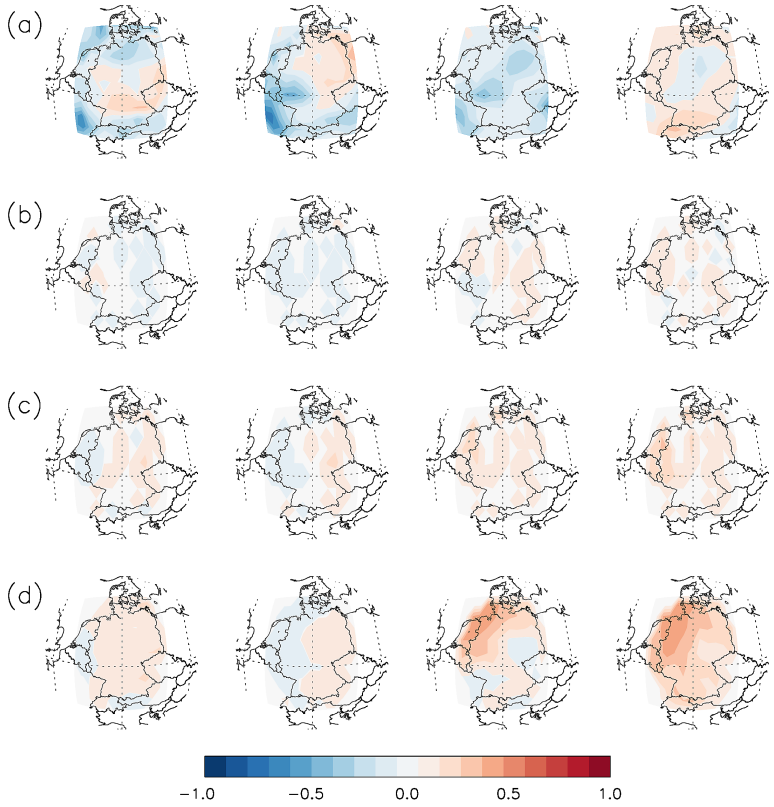

Figure S22: MSESS of seasonal PR GFCS2.1 hindcasts initialized in September. (a) ensemble mean; (b) ensemble mean downscaled with EOF teleconnctions; (c) subensemble mean based on empirical prediction of T2M-targeted teleconnections, downscaled with untargeted teleconnections; (d) subensemble mean based on empirical prediction of T2M-targetd teleconnections, downscaled with PR-targeted teleconnections. Left to right: lead times SON to DJF.

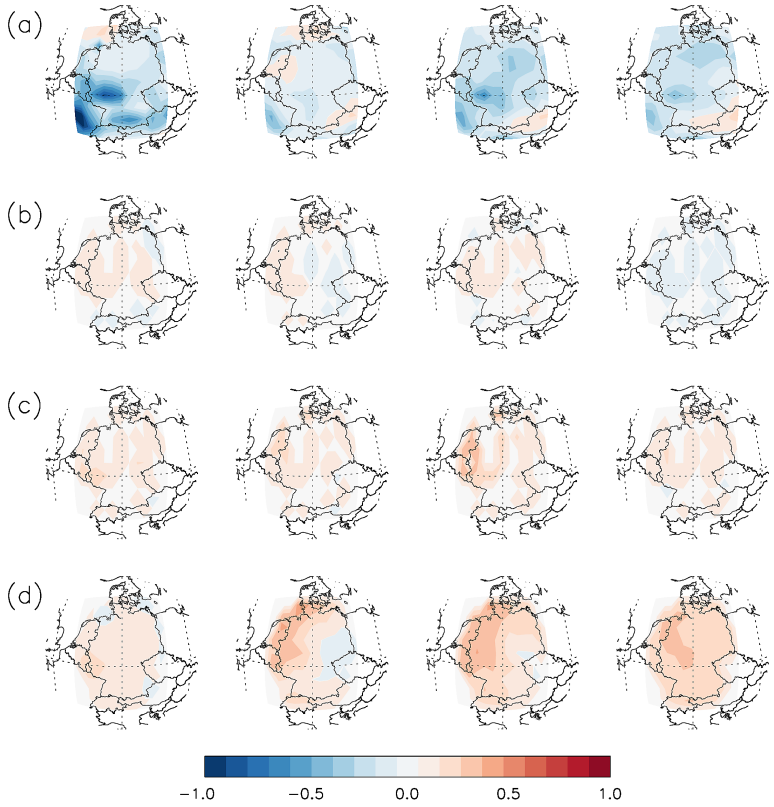

Figure S23: MSESS of seasonal PR GFCS2.1 hindcasts initialized in October. (a) ensemble mean; (b) ensemble mean downscaled with EOF teleconnctions; (c) subensemble mean based on empirical prediction of T2M-targeted teleconnections, downscaled with untargeted teleconnections; (d) subensemble mean based on empirical prediction of T2M-targetd teleconnections, downscaled with PR-targeted teleconnections. Left to right: lead times OND to JFM.

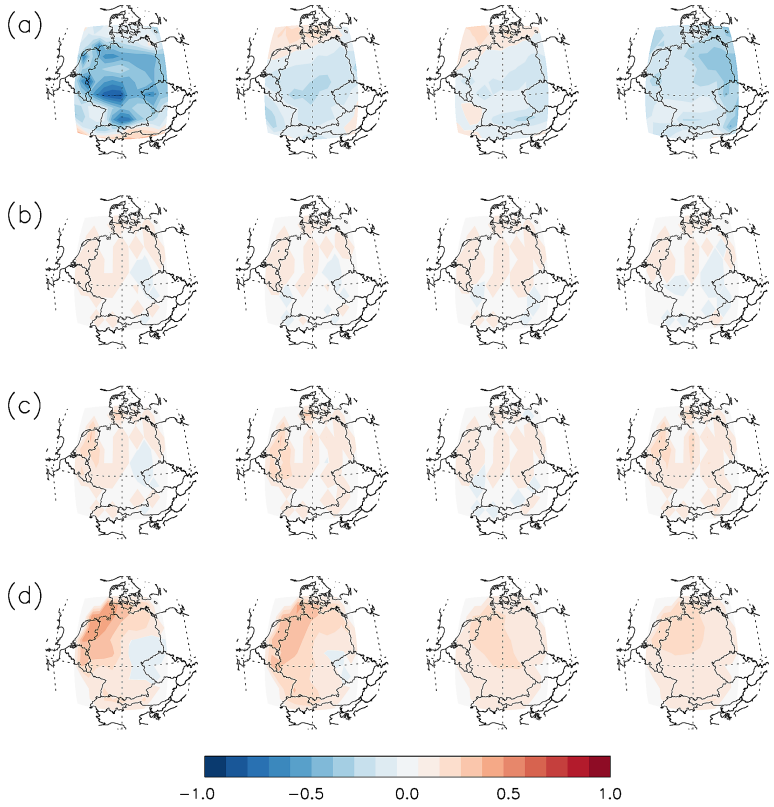

Figure S24: MSESS of seasonal PR GFCS2.1 hindcasts initialized in November. (a) ensemble mean; (b) ensemble mean downscaled with EOF teleconnctions; (c) subensemble mean based on empirical prediction of T2M-targeted teleconnections, downscaled with untargeted teleconnections; (d) subensemble mean based on empirical prediction of T2M-targetd teleconnections, downscaled with PR-targeted teleconnections. Left to right: lead times NDJ to FMA.

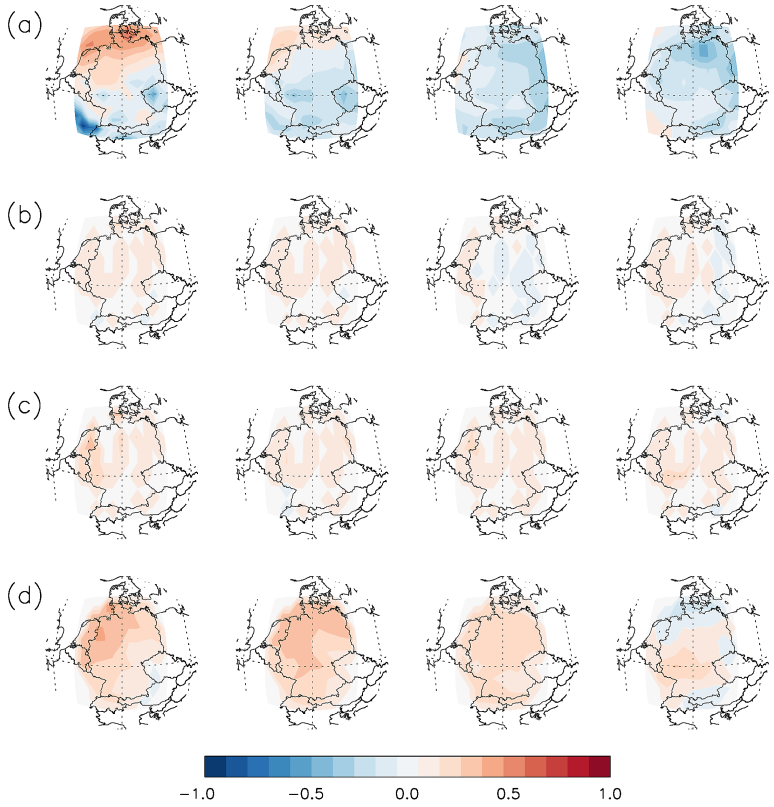

Figure S25: MSESS of seasonal PR GFCS2.1 hindcasts initialized in December. (a) ensemble mean; (b) ensemble mean downscaled with EOF teleconnctions; (c) subensemble mean based on empirical prediction of T2M-targeted teleconnections, downscaled with untargeted teleconnections; (d) subensemble mean based on empirical prediction of T2M-targetd teleconnections, downscaled with PR-targeted teleconnections. Left to right: lead times DJF to MAM.

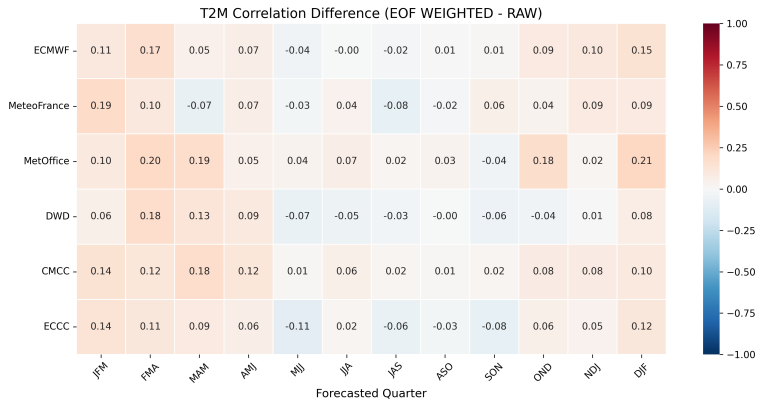

Figure S26: Differences in T2M skill between the ensemble weighted using EOFs and the RAW one. Each box represents de averaged difference of Spearman Rank correlation (computed between ensemble mean and ERA5 anomalies for each grid point, and for each of the ensembles) over the domain between 36° and 44° N, 9° W and 3° E. Each row represents a model, and each column the forecasted season, for a forecast initialized the month before. Red values indicate weighted ensemble outperforms raw ensemble.

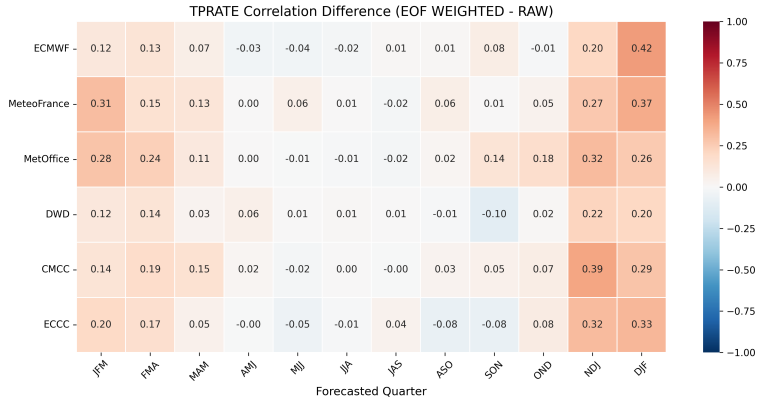

Figure S27: Same as Figure S26, but for PR

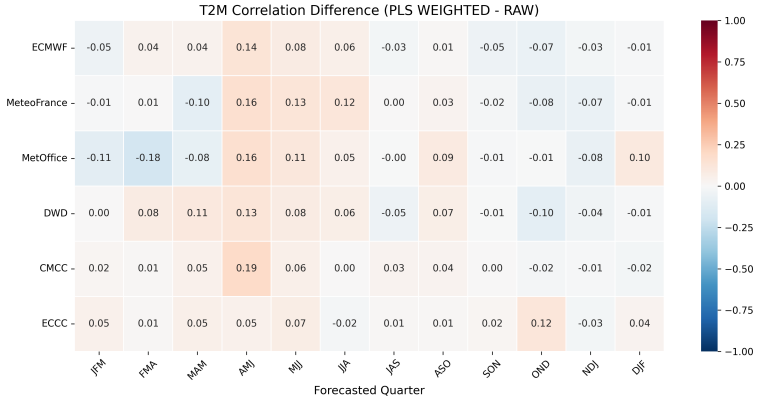

Figure S28: Same as figure S26, but using PLS modes instead of EOF

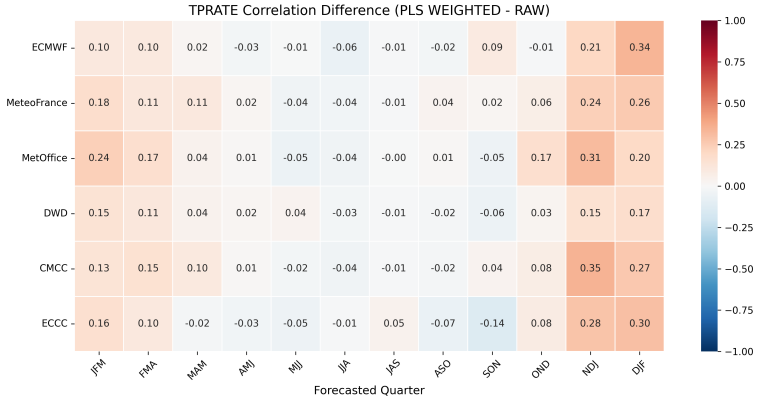

Figure S29: Same as Figure S28, but for PR